Powder Technology 411 (2022) 117873

Contents lists available at ScienceDirect

Powder Technology

journal homepage: www.journals.elsevier.com/powder-technology

Synthetic aperture rainbow refractometry for droplet refractive index and size measurement with long range: Standard and global modes

Yingchun Wu [a,b], Xinhao Wang [a,b], Dongyan Xu [a], Xuecheng Wu [a,*]

[a] State Key Laboratory of Clean Energy Utilization, Zhejiang University, Hangzhou 310027, China
[b] Huzhou Institute of Zhejiang University, Huzhou 313000, China

HIGHLIGHTS

- Synthetic aperture rainbow refractometry for long distance droplet measurement.
- SASRR measures mono-dispersed droplets at 1650 mm distance.
- SAGRR measures refractive index and size of spray with high accuracy.

GRAPHICAL ABSTRACT

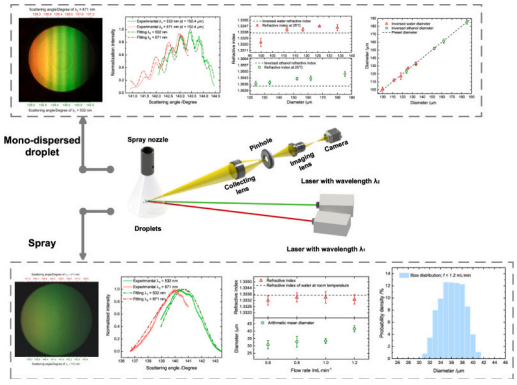

ARTICLE INFO

Keywords:
Rainbow refractometry
Spray
Long distance
Refractive index
Size

ABSTRACT

Optical characterizations of droplets and sprays at a long stand-off distance are of great demand in large scale facilities. Synthetic aperture rainbow refractometry (SARR) is proposed for long range measurement. The aperture of the imaging system is enlarged via synthesizing rainbow signals of the same droplet illuminated by multiple crossing laser beams from different channels of a color image simultaneously. The formation of the synthetic aperture rainbow signal is modeled by taking spectral response into account, and the retrievals of true rainbow signals are proposed. Both synthetic aperture standard rainbow refractometry (SASRR) and synthetic aperture global rainbow refractometry (SAGRR) are investigated, with corresponding inversion algorithms, and then validated with simulations and experiments. The uncertainties of refractive index and size of mono-dispersed droplet measured with the SASRR are 8×10^{-4} and 3 μm at 1650 mm distance, and for sprays measured with the SAGRR the deviation of refractive index is 8×10^{-4}. The proposed synthetic aperture rainbow refractometry enables transparent and spherical droplets and sprays measurement at long distance, and have great potential for large scale industrial applications.

* Corresponding author.
E-mail address: wuxch@zju.edu.cn (X. Wu).

https://doi.org/10.1016/j.powtec.2022.117873
Received 12 June 2022; Received in revised form 31 July 2022; Accepted 22 August 2022
Available online 27 August 2022

1. Introduction

Sprays and dispersed phases exist in numerous engineering applications, such as fuel injection in engine, herbicides in agriculture, spray freezing and drying, pharmaceutical spray, so investigation about atomization and spray procedures is of great practical significance. Measurement techniques [1] basically take important parts of spray investigation. In general the mathematical models of numerical simulation [2,3] require accurate data to adjust internal parameters, in order to constantly optimize and develop models to describe actual spray process more accurately. There is an urgent demand for dependable techniques for spray measurement [4,5], among which the laser diagnostic is evolving into the predominant instrument, taking the advantages of non-intrusive and in situ measurement. Given liquid instability, turbulence, cavitation and more, sprays have extensive random behaviors and every droplet may have different diameters and velocities, accompanied with droplet collision, fragmentation and fusion. Whether for the instantaneous spray such as fuel injection of aircraft engines [6,7] or for the steady atomization field like spray paint, spray characteristics measurement is carried out with high level of spatial and temporal resolution, great precision and repeatability. Laser diagnostic techniques can meet the above and have no affect on the original flow field. Laser diagnostic has been applied extensively and taking a unique part in engineering applications. However, the measuring distance of laser diagnostics in the laboratory cannot satisfy large scale industrial scenes like the simulated cloud field in the icing wind tunnels [8,9]. It needs to be addressed in advance that the difficulties and challenges caused by long measurement distance, disturbances and restricted space, in order to comprehensively utilize laser diagnostic in industrial droplet measurement.

Nowadays, the available laser diagnostic techniques focus on flow field, temperature, velocity, droplet size, mass distribution, concentration, etc., and most of those have been developed to large scale applications. As one of the most important parameters, droplet size greatly determines spray applicability, and interferometric particle imaging (IPI) [10] is an effective approach to measure droplet size, also competent for more dense sprays and flow field with higher resolution and acquisition rate. The IPI had been continuously applied to long range measurement [11] with distance of 1600 mm and 2290 mm. High-speed imaging [12] enables to opportunely capture specific observations and completely view the evolution of certain processes besides droplet size. For three dimensional (3D) droplet size measurement, digital holography (DH) [13,14] takes the advantage of real three dimensional (3D) imaging, obtaining 3D position and velocity. The long distance investigations of holography were available [15] over several kilometres, and an experiment with distance from the observatory to the target of approximately 1.2×10^7 mm was carried out at the U.S. Air Force Electro-Optics Facility. Phase Doppler interferometry/anemometry (PDI/PDA) [16] can also achieve droplet size and velocity measurement, based on the laser Doppler anemometry (LDA), but limited to single point measurement. A 2D-LDV long range optics was designed for applications which needed a longer-than-usual focal length to access the measurement area 2000 mm and far away [17]. Among these, rainbow refractometry is a distinctive approach for size, refractive index (RI) and RI-related parameters measurement in the backscattered region. Most investigations of rainbow refractometries are increasing dimensions, more parameters and applicable to non-spherical droplets. While Roth et al. [18] initially presented a droplet measurement technique using rainbow theory, which was the standard rainbow refractometry (SRR), Van Beeck et al. [19] increased the range of measurement area and reduced sampling frequency to make rainbow refractometry applied to sprays, named the global rainbow refractometry (GRR). Subsequently for spherical droplets on a line, Wu et al. [20] proposed one-dimensional rainbow refractometry and then Li et al. [21] is capable to describe droplet size and refractive index of sprays on a specific surface by planar rainbow refractometry. Wu et al. proposed phase rainbow refractometry to capture the nanoscale variation of droplet size [22], and used global rainbow refractometry to measure mixing ratio in multiple sprays [23]. The surface tension and viscosity of the oscillating droplet were surveyed using rainbow refractometry by Lv et al. [24]. As for non-spherical droplet, Saengkaew et al. [25] quantified the accuracy of non-spherical droplet measurement using rainbow refractometry after the detection method was suggested [26], and Yu et al. [27] developed a model to simulate optical caustic structures of the oblate droplets. However, most applications like large scale icing wind tunnels [28] need available focal length with at least 1500 mm, from wall to core of the test section. Rainbow refractometry can be located outside the tunnel and requires only an optical window on one side of the wall. Rainbow refractometry not only measure droplet size, refractive index, temperature, composition and so on simultaneously, but also achieve accurate and realistic droplet measurement without disrupting internal flow field. But the measuring distance of existing rainbow refractometry is limited to several hundred millimeters. It is impossible for rainbow refractometry to measure droplets in the middle of the test section. So there are urgent and significant requirements of rainbow refractometry with long measurment distance.

Therefore, this work proposed synthetic aperture rainbow refractometry for refractive index and size measurement of transparent and spherical droplet at long distance. At first, principle of the synthetic aperture rainbow refractometry and an model about extracting light intensity from color image are presented in Section 2. And then the inversion algorithm, simulation and experiments of synthetic aperture standard rainbow refractometry are proposed to prove the feasibility and accuracy of the technique in Section 3. Finally, the synthetic aperture global rainbow refractometry is used to measure dispersed droplets, which achieves rainbow refractometry for long distance spray measurement in Section 4.

2. Principle

The rainbow refractometry records light distribution and angular position of the main peak from rainbow signal, which is sensitive to droplet refractive index (RI) and size, to achieve droplet measurement. The complete main peak of rainbow signal must be captured and imaged on the camera for data inversion with high precision, in other words, the aperture of the imaging system should cover the scattering angle of the first Airy peak. The scattering angle of rainbow lobes is relative to droplet refractive index and size. According to the first zero point of the Airy function [29] in the range of variables less than 0, the relationship can be expressed as

$$\theta_f - \theta_{rb} = \frac{816}{349} \frac{(4-n^2)^{\frac{1}{6}}}{(n^2-1)^{\frac{1}{2}}} \left(\frac{3}{\lambda d}\right)^{\frac{2}{3}}, \tag{1}$$

where n is the refractive index of droplet, λ is the laser wavelength and d is the droplet diameter. θ_{rb} is the geometric rainbow angle. θ_f is a special angle where the light intensity is minimal in the range from the main peak to the first supernumerary bow. The minimum angle of the complete main peak of rainbow signal is considered that the value of Airy function is 0.1, and the maximum angle is θ_f. The width of the complete main peak is approximately $\frac{4}{3}(\theta_f - \theta_{rb})$. Fig. 1 demonstrates the relationship of $\theta_f - \theta_{rb}$ with refractive index and diameter, and the difference of angle varies widely with droplet size especially less than 100 μm. The variation of $\theta_f - \theta_{rb}$ is small with refractive index, but the absolute position of the scattering angle would move. Thus, the measurement distance of the rainbow refractometry is mainly restricted by the collecting lens, droplet refractive index and diameter. For large scale industrial applications, a straightforward approach is to increase the lens size of the imaging system. However, this way would encounter large volume of apparatus and serious spherical aberration, deteriorating the signal noise ratio. And common lens with size of up to 4 inches

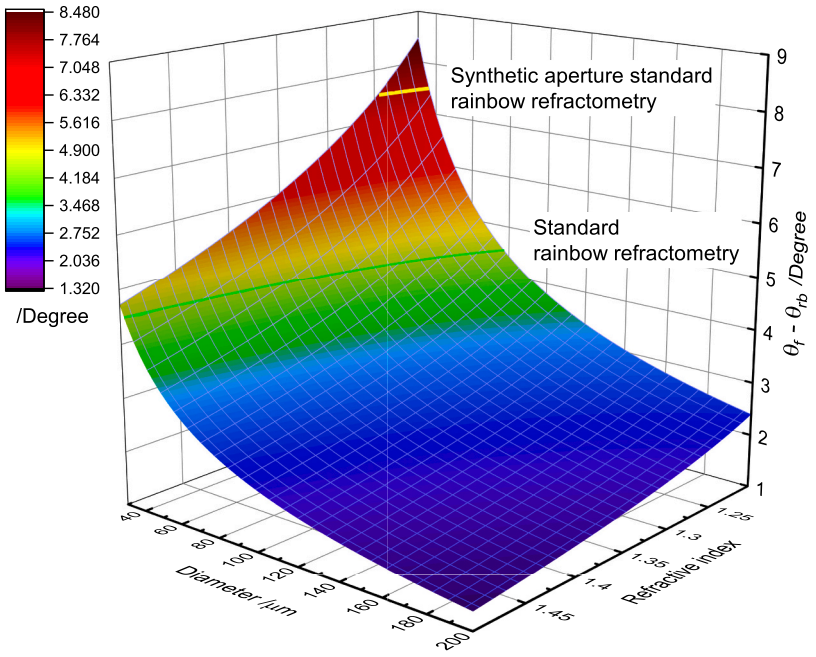

Fig. 1. The relationship of $\theta_f - \theta_{rb}$ with refractive index and size, and the measurement range of standard rainbow refractometry and synthetic aperture standard rainbow refractometry.

is difficult to accommodate partial industrial applications.

Inspired by rainbow in nature and large view field measurement provided by synthetic aperture radar [30], the rainbow refractometry for large scale applications can be achieved by synthesizing aperture. Laser beams with different wavelengths are used to illuminate droplets at different incident angles. After scattered by the droplet, fractional rainbow signals are generalized. The rainbow signals from all the laser beams are recorded simultaneously in different channels of color camera and then synthesized to a full rainbow signal for procession. The equivalent aperture is enlarged in this way, and it is capable for large view and long distance measurement. Thus, this method is named the synthetic aperture rainbow refractometry (SARR). The light path and principle of the synthetic aperture rainbow refractometry are shown in Fig. 2. Here is an example to illustrate the advantages of the SARR for long distance measurement, and the experimental objects are lens of 4 inches and measurement distance of 700 mm. The aperture of original rainbow refractometry will be 6° or less if taking spherical aberration of lens and fluctuation of droplet parameters into account, and the $\theta_f - \theta_{rb}$ is 4.5°. Whereas the equivalent aperture of the SARR is about 10° considering one third of the overlapping area, and the $\theta_f - \theta_{rb}$ is 7.5°. Through simulation by the Lorenz-Mie theory [31], the measurement ranges of refractive index and size with the same imaging system for standard rainbow refractometry and synthetic aperture rainbow refractometry are displayed in Fig. 1. The parts below the yellow and green curves are where the SARR and the standard rainbow refractometry can measure. The coverage area of the SARR is significantly larger than the original rainbow refractometry. The SARR not only achieves long distance measurement with small volume, but also eliminates setting an additional laser beam to mark the measurement area during calibration.

While capturing rainbow signals in different channels of industrial color camera, interference between laser beams with different wave-

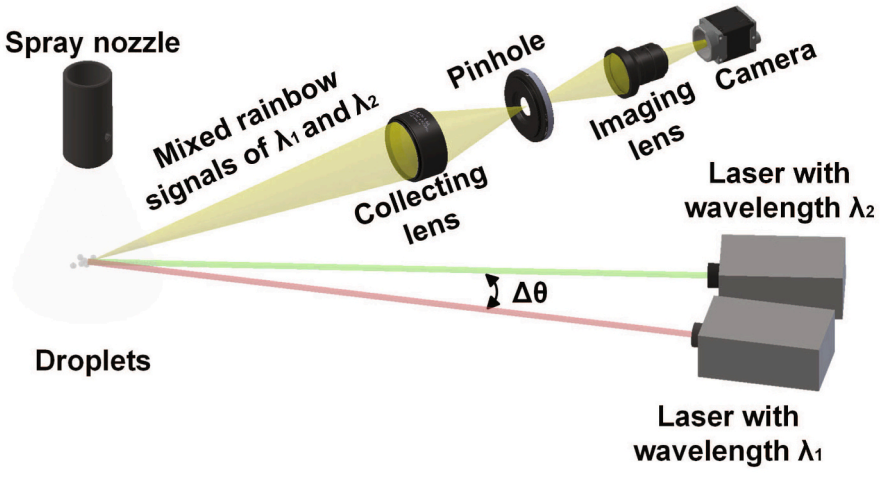

Fig. 2. The optical path and principle of the synthetic aperture rainbow refractometry.

lengths would influence light intensity for procession. A method is proposed to eliminate such interference as much as possible. The signals recorded by camera are distributed in three different channels of a color image, named R, G and B here. The signal of an image is expressed as

$$\mathbf{I}_{\text{img}} = \begin{bmatrix} \mathbf{I}(\text{R}) \\ \mathbf{I}(\text{G}) \\ \mathbf{I}(\text{B}) \end{bmatrix} = \begin{bmatrix} \text{C}_{\text{R1}}, \text{C}_{\text{R2}} \\ \text{C}_{\text{G1}}, \text{C}_{\text{G2}} \\ \text{C}_{\text{B1}}, \text{C}_{\text{B2}} \end{bmatrix} \times \begin{bmatrix} \mathbf{I}_{\text{img}}(\lambda_1) \\ \mathbf{I}_{\text{img}}(\lambda_2) \end{bmatrix}, \tag{2}$$

where λ_1 and λ_2 are the wavelengths of laser beams. $\text{C}_{\text{R1}}, \text{C}_{\text{R2}}$ represent the coefficient of spectral response for channel R to λ_1 and λ_2 respectively, and $\text{C}_{\text{G1}}, \text{C}_{\text{G2}}$ and $\text{C}_{\text{B1}}, \text{C}_{\text{B2}}$ are that of the channel G and B. According to the spectral response of camera [32], the signal of λ_1 is mainly stored in the channel G, and the signal of λ_2 is in the channel R, which means C_{G1} and C_{R2} values are much larger than other coefficients. Each channel records signals of both lasers, so it is impossible to obtain the light intensity of a laser only by exporting signal from the corresponding channel. The correction experiment is to capture rainbow signals of λ_1 and λ_2 laser beams by camera, and the signal is

$$\mathbf{I}_{\lambda_i} = \begin{bmatrix} \mathbf{I}(\text{R}) \\ \mathbf{I}(\text{G}) \\ \mathbf{I}(\text{B}) \end{bmatrix} = \begin{bmatrix} \mathbf{I}_{\text{R}}(\lambda_i) \\ \mathbf{I}_{\text{G}}(\lambda_i) \\ \mathbf{I}_{\text{B}}(\lambda_i) \end{bmatrix}, \tag{3}$$

where the subscript $i = 1,2$ represent different laser beams. In this way, the light intensity of λ_i recorded in other channels of camera is obtained, and the light intensity of λ_1 and λ_2 can be expressed as

$$\begin{cases} \mathbf{I}_{\text{SA}}(\lambda_1, \theta) = \text{C}_{\text{G1}}\mathbf{I}_{\text{img}}(\lambda_1) + \text{C}_{\text{G2}}\mathbf{I}_{\text{img}}(\lambda_2) - \mathbf{I}_{\text{G}}(\lambda_2), \\ \mathbf{I}_{\text{SA}}(\lambda_2, \theta) = \text{C}_{\text{R1}}\mathbf{I}_{\text{img}}(\lambda_1) + \text{C}_{\text{R2}}\mathbf{I}_{\text{img}}(\lambda_2) - \mathbf{I}_{\text{R}}(\lambda_1). \end{cases} \tag{4}$$

Thus, the light intensity distribution of each laser without interference is obtained.

3. Synthetic aperture standard rainbow refractometry

3.1. Inversion algorithm

In order to verify the feasibility of the synthetic aperture standard rainbow refractometry (SASRR), inversion algorithm, numerical simulation and validation experiment are described in this section. The relationship between light scattering angle and camera pixel is obtained by mirror calibration. $\theta_{\min}$ and $\theta_{\max}$ are the minimum and maximum values of scattering angle for the laser beam λ_1, and $\Delta\theta$ represents angle of two light scattering λ_1 and λ_2 as shown in Fig. 2. Two superimposed signals can be expressed as $\mathbf{I}(\lambda_1, \boldsymbol{\theta}_1)$ and $\mathbf{I}(\lambda_2, \boldsymbol{\theta}_2)$, where $\boldsymbol{\theta}_1 \in [\theta_{\min}, \theta_{\max}]$, $\boldsymbol{\theta}_2 \in [\theta_{\min} - \Delta\theta, \theta_{\max} - \Delta\theta]$. During experiment, the synthetic aperture standard rainbow signals are stored in different channels of a color image, so the light intensity distribution is

$$\mathbf{I}_{\text{SA}}(\lambda, \theta) = \mathbf{I}(\lambda_1, \boldsymbol{\theta}_1) + \mathbf{I}(\lambda_2, \boldsymbol{\theta}_2). \tag{5}$$

Considering droplets are homogeneous, transparent and spherical, the hypothetical synthetic aperture standard rainbow signals can be obtained through rainbow theories, among which the complex angular momentum (CAM) theory [29,33] is accurate and short time-consuming and thus used in this work. The hypothetical light intensity of rainbow signal is

$$\mathbf{I}_{\text{fit}}(\lambda, \theta, d) = c_1\mathbf{I}_{\text{fit}}(n_{\lambda_1}, \boldsymbol{\theta}_1, d) + c_2\mathbf{I}_{\text{fit}}(n_{\lambda_1} - \Delta n, \boldsymbol{\theta}_2, d), \tag{6}$$

where droplet size d and refractive index n are the values to be solved. c_1 and c_2 are the coefficients to eliminate the impact of unequal light intensity of two laser beams. Because of chromatic dispersion, the refractive indices of different laser beams are different for the same droplet, and Δn represents gap between the RI values of λ_1 and λ_2 laser beams. The relationship formulas are different for water and ethanol, and the Sellmeier formula [34] can predict water refractive index of different wavelengths with high accuracy, which is

$$\Delta n = \sqrt{1 + \frac{A_1\lambda_1^2}{\lambda_1^2 - B_1} + \frac{A_2\lambda_1^2}{\lambda_1^2 - B_2}} - \sqrt{1 + \frac{A_1\lambda_2^2}{\lambda_2^2 - B_1} + \frac{A_2\lambda_2^2}{\lambda_2^2 - B_2}}. \tag{7}$$

The Cauchy equation [34] can be used for ethanol refractive index as

$$\Delta n = \sqrt{C_0 + \frac{C_1}{\lambda_1^2} + \frac{C_2}{\lambda_1^4} + C_3\lambda_1^2} - \sqrt{C_0 + \frac{C_1}{\lambda_2^2} + \frac{C_2}{\lambda_2^4} + C_3\lambda_2^2}. \tag{8}$$

The exact values of coefficients $A_1, A_2, B_1, B_2, C_0, C_1, C_2$ and C_3 refer to the literature [34]. Non-negative least squares method (NNLS) is adopted to gain the only positive solution of n and d values by finding $\mathbf{I}_{\text{fit}}(\lambda, \theta, d)$ optimally close to $\mathbf{I}_{\text{SA}}(\lambda, \theta)$, and the iterative optimization objective can be expressed as

$$\underset{n,d}{\text{argmin}}\left\{\left|\mathbf{I}_{\text{SA}}(\lambda, \theta) - \mathbf{I}_{\text{fit}}(\lambda, \theta, d) - \mathbf{I}_{\text{Noise}}\right|\right\}, \tag{9}$$

where $\mathbf{I}_{\text{Noise}}$ is the light intensity of noise. It is more efficient and accurate while providing the initial ranges of $n_{\lambda 1}$ and $d, n_{\lambda 1} \in [n_{\min}, n_{\max}]$ and $d \in [d_{\min}, d_{\max}]$, for searching the minimum value of Eq. (9).

3.2. Simulation validation

In order to validate the feasibility and precision of the SASRR from numerical simulation, the synthetic aperture standard rainbow signals are simulated by the Lorenz-Mie theory and inversed. RI and droplet size are changed during simulation, avoiding randomness in conclusions. The RI values are $n_{\lambda 1} = 1.3337$ and 1.3637 and the droplet size values are $d = 50\ \mu$m, 75 μm, 100 μm, 125 μm and 150 μm. The simulated synthetic aperture standard rainbow signal of $d = 100\ \mu$m, $n_{\lambda_1} = 1.3337$ is exhibited in the solid lines of Fig. 3(a), and it is obvious that the position of rainbow main peak moves for different laser beams. The $\lambda_2 =$ 671 nm curve offers information from the Alexander's dark band to the main peak, 135.8° to 139.2°, which involves the geometric rainbow angle. The light scattering from the main peak to the first supernumerary bow is intercepted by the $\lambda_1 = 532$ nm curve from 138.5° to 142.0°. In other words, the synthetic aperture standard rainbow signal combines two fractional rainbow signals from the wavelength of 532 nm and 671 nm, covering from the dark band to the first supernumerary bow, sufficient for droplet RI and diameter inversion.

The simulated signals are processed by the inversion algorithm mentioned above, and the results can prove the reliability of the SASRR. The dotted lines in Fig. 3(a) is the fitting of the synthetic aperture standard rainbow signals, and all curves stay consistent. The RI and size values are demonstrated in Fig. 3(b) and (c) respectively and the comparisons with preset values are also reflected. For inversion of refractive index, the mean deviation is 7×10^{-4} and results from $n_{\lambda_1} = 1.3337$ of different sizes indicates the change of droplet size has no effect on the RI. The uncertainties of water and ethanol droplet sizes are both within 2 μm and different RI cannot influence diameter values.

3.3. Experimental verification

Experimental setup of the SASRR involved a laser beam generation unit and an imaging system. The laser beam generation unit was mainly two lasers with different wavelengths of 532 nm and 671 nm and straightening element. The maximum power of two lasers was 2.5 W ensuring adequate intensity of light scattering for long distance measurement. The imaging system was composed of a collecting lens, a pinhole, an imaging lens and a color industrial camera as displayed in Fig. 2. Both lens were achromatic in order to eliminate dispersion and chromatic aberration, and avoid movement of focusing surface caused by different laser beams. The color industrial camera was Basler acA2040-90uc with sensor size of 11.3 mm × 11.3 mm, and it recorded different color signals with different channels. According to the spectral response properties of the camera [32], the gap of quantum efficiency

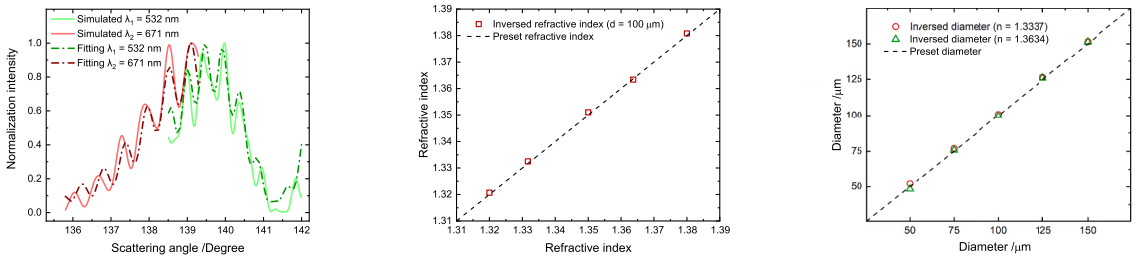

(a) (b) (c)

Fig. 3. (a) The simulated synthetic aperture standard rainbow signal and the fitting curves with wavelength of $\lambda_1 = 532$ nm and $\lambda_2 = 671$ nm ($d = 100$ μm, $n_{\lambda_1} = 1.3337$). (b) The inversed and preset refractive index values of $\lambda_1 = 532$ nm with $d = 100$ μm. (c) The inversed and preset diameter values of $n_{\lambda_1} = 1.3337$ and $n_{\lambda_1} = 1.3634$.

between $\lambda_1 = 532$ nm and $\lambda_2 = 671$ nm is large, and the interference is reduced in the Eq. (4). A mirror was adopted to calibrate the relationship of scattering angle and camera pixel. It was more convenient because measurement point was the intersection of two laser beams without an additional locating device. Mono-dispersed droplet streams of water and ethanol were produced by a self-developed mono-dispersed droplet stream generator (MDSG), which can control droplet size through adjusting flow rate, vibration frequency and nozzle size. The droplet temperature was controlled through keeping the temperature constant and balanced in the laboratory.

The synthetic aperture standard rainbow refractometry was used to measure mono-dispersed spherical droplets at the distance of 1650 mm with different RI and diameters. Fig. 4(a) and (b) display two typical synthetic aperture standard rainbow images of water and ethanol droplet. The ripple structures of rainbow signal can be observed and the green and red light distribute on both sides with yellow light located in the mid-ground. Taking the average and then normalizing 200 rows of pixels in the middle of rainbow images, the normalization synthetic aperture standard rainbow light intensity is obtained and demonstrated in the solid lines of Fig. 4(c). $\lambda_1 = 532$ nm curve is from 142° to 144.5°, covering from the main peak to the first supernumerary bow, while $\lambda_2 = 671$ provides rainbow signal from the Alexander's dark band to the main

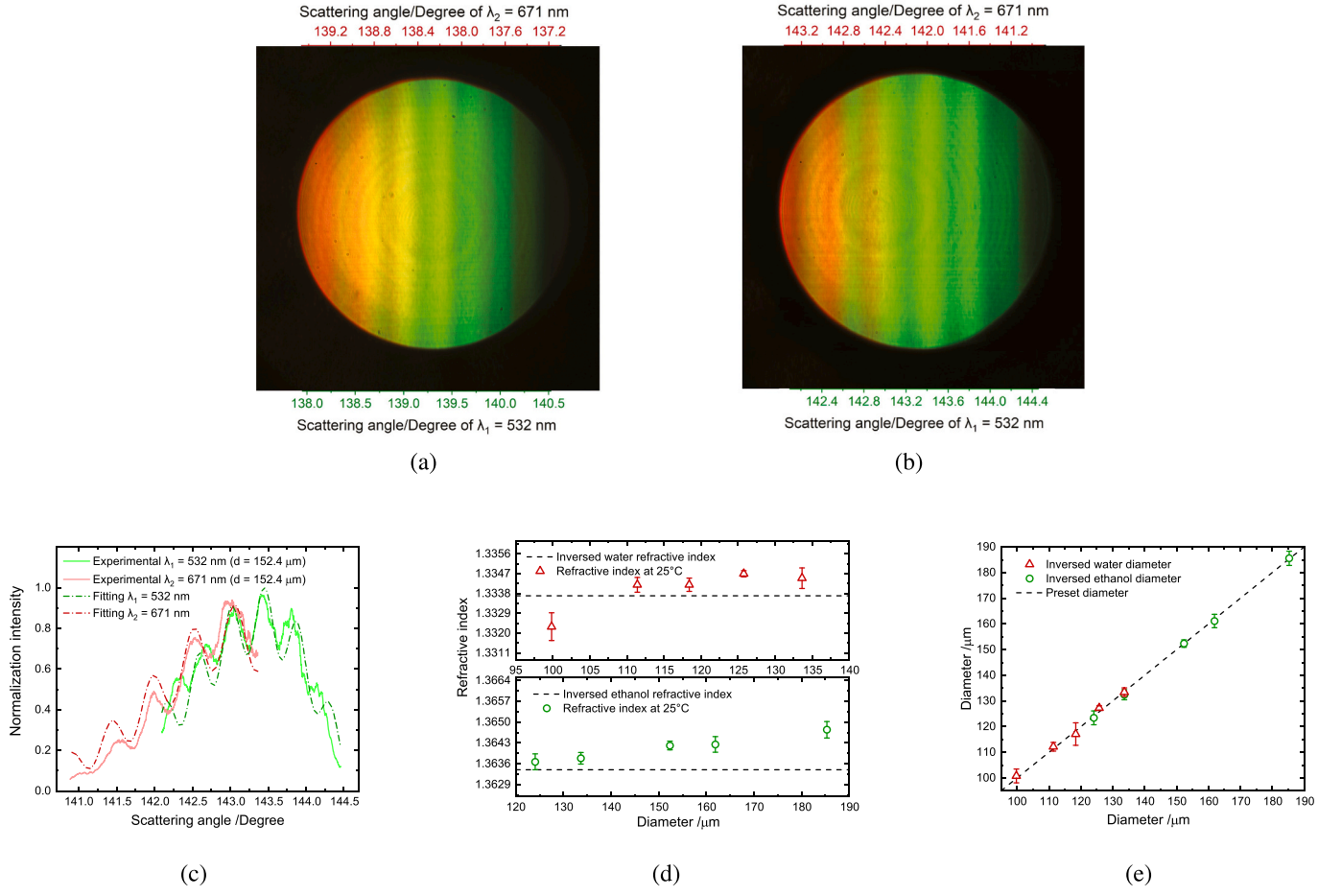

(a) (b) (c) (d) (e)

Fig. 4. (a) The synthetic aperture standard rainbow image of mono-dispersed water droplet with $d = 118.4$ μm. (b) The synthetic aperture standard rainbow image of mono-dispersed ethanol droplet with $d = 152.4$ μm. (c) The normalization light intensity distribution of synthetic aperture standard rainbow signal and the fitting in Fig. 4(a). (d) The inversed and preset refractive index values of $\lambda_1 = 532$ nm, and the top is water droplets and the bottom is ethanol droplets. (e) The inversed and preset diameter values of water and ethanol droplets.

peak, 141° to 143.5°. The aperture of system allowes around 2.5° light scattering passage with a laser beam, but it achieves droplet measurement with size about 150 μm at 1650 mm distance as the SASRR.

The fitting of synthetic aperture standard rainbow signal is exhibited in the dotted lines of Fig. 4(c) and the performance of fitting curves guarantees the accuracy of data procession. Water and ethanol RI values from the SASRR of $\lambda_1 = 532$ nm is 1.3340 and 1.3641 respectively, while the corresponding refractive indices from the reference [35,36] are 1.3337 and 1.3634 at room temperature. As demonstrated in Fig. 4(d), the inversed RI values of different diameters are close to the standard values for both water and ethanol. The uncertainties are 8×10^{-4} and 7×10^{-4} for water and ethanol respectively, fulfilling the requirements of engineering application. It can be noticed from Fig. 4(d) the change of droplet size has no effect on the RI measurement. Five different droplet sizes of water and ethanol were measured by the SASRR, and results were compared with that of MDSG, whose diameters have been certified [37]. Fig. 4(e) illustrates the diameter of water and ethanol droplets with preset diameter. The deviations of all ten working conditions are within 3 μm, with high accuracy and stability. It is proved the synthetic aperture standard rainbow refractometry can be used to measure mono-dispersed spherical droplets with 1650 mm distance. Combined with the above mentioned large icing wind tunnels, the measurement distance should be at least 1500 mm and the supercooled large droplets have size of more than 100 μm. It is certified that the synthetic aperture rainbow refractometry can be applied to the real scale industrial applications.

In order to highlight the strength and superiority of the SASRR, two comparison experiments are introduced. The monochrome fractional rainbow signals of $\lambda_1 = 532$ nm and $\lambda_2 = 671$ nm are inversed separated from the synthetic aperture standard rainbow signals, and the maximum measurement distance of a laser beam is surveyed with the same imaging system as the SASRR. The former comparative experiment obtains the rainbow signals of 532 nm and 671 nm from the synthetic aperture standard rainbow images, and processes these with the inversion algorithm of standard rainbow refractometry. With the same preset parameters as the SASRR, inversed RI and diameters of $d = 152.4$ μm are displayed in Fig. 5. Fig. 5(a) and (b) are the fitting of experimental rainbow signals from $\lambda_1 = 532$ nm and $\lambda_2 = 671$ nm, but there are more obvious gaps compared with Fig. 4(c). Inversed diameter values from dual-wavelength and two single laser beams of the same images are shown in Fig. 5(c), and the black line represents diameter value from the MDSG. The diameter procession of $\lambda_1 = 532$ nm performs better than that of 671 nm, but the accuracy is lower than the SASRR. The RI of 532 nm is 1.3639 close to 1.3634 at room temperature. It is presumed the signals of $\lambda_1 = 532$ nm accounts for more region of the complete rainbow signal, so the fitting is better especially the orientation of the main peak. Due to the absence of the dark band, the fitting curve was widen than the experimental curve, leading to lower diameter values. The results of $\lambda_2 = 671$ nm have more errors on the fitting situation, RI and diameter. The fitting curve of 671 nm is narrower than that from experiment, so the diameter is larger than SASRR. The latter comparative experiment is that the measuring distance is adjusted to survey the same droplet with the same system but a laser beam, and the measuring distance is 1100 mm. In conclusion, it is necessary and meaningful to develop the synthetic aperture rainbow refractometry.

4. Synthetic aperture global rainbow refractometry

4.1. Inversion algorithm

The synthetic aperture standard rainbow refractometry introduced above can measure mono-dispersed spherical droplets, and there is a great requirement for spray measurement with long distance. Therefore, the synthetic aperture global rainbow refractometry (SAGRR) is presented in this section. The inversion algorithm, numerical simulation and validation experiment need to be adjusted for poly dispersed spherical droplets. The synthetic aperture global rainbow signals of experiment can be expressed in the form of

$$\mathbf{I}_{\mathrm{SA}}(\lambda, \theta, d) = \mathbf{I}(\lambda_1, \boldsymbol{\theta}_1, d) + \mathbf{I}(\lambda_2, \boldsymbol{\theta}_2, d). \tag{10}$$

Assuming droplets are homogeneous, transparent and spherical, the scattering and interference among droplets are ignored. The light intensity distribution of droplet cloud is briefly stated as

$$\mathbf{I}_{\mathrm{fit}}(\lambda, \theta, d) = \sum_{m=1}^{M} \mathbf{I}(n_\lambda, \boldsymbol{\theta}, d_m) \cdot N(d_m), \tag{11}$$

where $N(d)$ is the probability density size distribution of droplet cloud and M is the number of droplet bins. The M is determined by dividing the droplet size range into several bins of about 5 μm each for high accuracy and little time consuming of procession. The Eq. (11) can be discrete to create a linear system of equation and combining with the Eq. (10). The hypothetical light intensity of the rainbow signal is

$$\begin{aligned}\mathbf{I}_{\mathrm{fit}}(\lambda, \theta, d) = c_1 \left[\mathbf{I}_{\mathrm{fit}}(n_{\lambda_1}, \boldsymbol{\theta}_1, d_1) \cdots \mathbf{I}_{\mathrm{fit}}(n_{\lambda_1}, \boldsymbol{\theta}_1, d_M)\right] \cdot \begin{bmatrix} N(d_1) \\ \vdots \\ N(d_M) \end{bmatrix} + c_2 \left[\mathbf{I}_{\mathrm{fit}}(n_{\lambda_1} \right. \\ \left. - \Delta n, \boldsymbol{\theta}_2, d_1) \cdots \mathbf{I}_{\mathrm{fit}}(n_{\lambda_1} - \Delta n, \boldsymbol{\theta}_2, d_M)\right] \cdot \begin{bmatrix} N(d_1) \\ \vdots \\ N(d_M) \end{bmatrix},\end{aligned} \tag{12}$$

where Δn of water and ethanol are calculated from the Eqs. (7) and (8), and the I_{fit} in the equation is calculated by the CAM. The optimal n_{λ_1} and $N(d)$ values are searched to satisfy the condition of Eq. (9) in the given ranges of $[n_{\min}, n_{\max}]$ and $[d_{\min}, d_{\max}]$. The probability density of droplet size in the range of $[d_{\min}, d_{\max}]$ can be obtained by $N(d)$, and the size distribution and the arithmetic mean diameter d_{A} are obtained after corresponding calculation. In this way, the RI and size distribution of droplet cloud would be inversed from the synthetic aperture global rainbow signals.

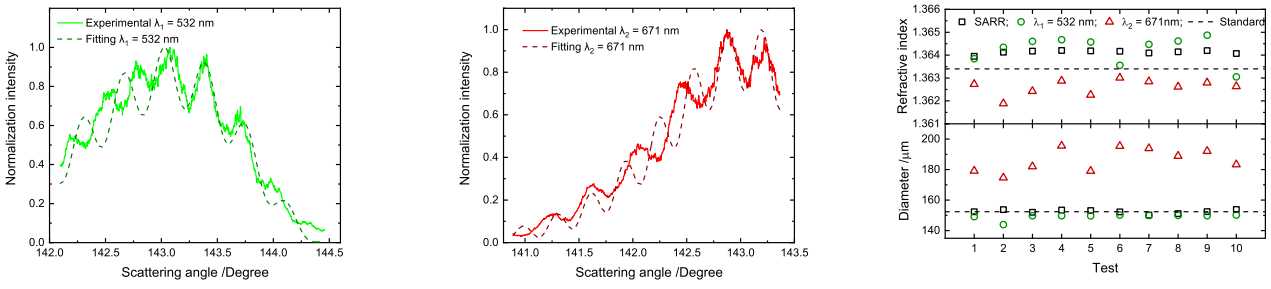

(a) (b) (c)

Fig. 5. (a) The fitting of experimental rainbow signal of $\lambda_1 = 532$ nm. (b) The fitting of experimental rainbow signal of $\lambda_2 = 671$ nm. (c) The inversed RI and diameter values from rainbow signals with dual-wavelength and two single laser beams.

4.2. Simulation validation

The synthetic aperture global rainbow signals of seven different size distributions and two different refractive indices were simulated, corresponding to that of water and ethanol, for the purpose of verifying the feasibility and accuracy of the SAGRR. Through the Lorenz-Mie theory, the global rainbow signals are acquired by superimposing multiple rainbow signals of mono-dispersed droplets which eliminate ripple structure. The simulated droplet size had the normal distributions, where the expectations of distribution, also the arithmetic mean diameters, d_A = 30 μm, 50 μm, 75 μm, 100 μm and 150 μm, and the standard deviations of $\delta = 5$ and 10. The solid lines of Fig. 6(a) show the simulated synthetic aperture global rainbow signals with d_A of 50 μm and RI of 1.3337, and the main peak is obvious without ripple structure.

The fitting of the simulated synthetic aperture global rainbow signal is shown in the dotted lines of Fig. 6(a), and the highly overlapping of two signals indicates the reliability of the SAGRR. After processing water rainbow signals of different size distributions, the RI values are stable with the mean deviation of 3×10^{-4} shown in Fig. 6(b). The inversed arithmetic mean diameters are 22.7 μm, 47.1 μm, 71.4 μm, 98.2 μm and 142.2 μm respectively, as Fig. 6(c) illustrates. The size distributions with the standard deviation of 5 μm and 10 μm are exhibited in Fig. 7(a) and (b) with the expectation of 50 μm. The general trend is close to the normal distribution, and the former is superior to the latter in terms of size distribution inversion. The comparisons of preset and inversed size distributions with the expectations of 50 μm and 75 μm are in Fig. 7(b) and (c). It is obvious that the percentage of smaller droplet size is higher, meaning the overall distribution is inclined towards smaller size. The possible factor of such errors is the fitting of λ_2 curve is predominant for the presence of geometric rainbow signals, but the fitting of λ_1 is mistake-prone. The fitting rainbow signals in Fig. 6(a) is wider than the simulated one, leading to the differences in Fig. 7. The droplets of different refractive indices with the same size distribution are simulated and inversed, and the size distribution ($d_A = 50$ μm, $\delta = 10$, $n = 1.3200$) is displayed in Fig. 7(d). It is shown the viable refractive index has no affect on size distribution inversion.

4.3. Experimental verification

There were adjustments of experimental layout to spray measurement. At first, the positions of the collecting lens and the imaging lens were calculated and searched for the Fourier imaging system. The key benefit of this imaging system is the light scattering with the same angle of different droplets in the measuring area is converged and imaged on the same point of camera target, which means the rainbow signals of different droplets can be averaged and displayed on the camera. And then the collecting lens and the pinhole helped removing background noise and controlling size of measuring area as a spatial filtering system. Lastly, the pinhole size was increased and the exposure time of camera was enlarged, ensuring one image can capture the average rainbow signals of droplets as many as possible. A nozzle could produce spray and the ratio of air to water was altered during the experiment. The variable ratio of air to water was achieved by controlling liquid flow rate. Mono-dispersed droplets with size of around 150 μm were measured by the SASRR, and in addition to hundred microns, droplets with tens of microns exist extensively in large scale applications like fuel injection of aircraft engines. In order to prove the feasibility for small droplets, the droplet size in spray was around 35 μm. Thus, the measurement distance of the SAGRR was up to 800 mm.

The spray is investigated by the synthetic aperture global rainbow refractometry, and droplet size and refractive index are inversed. The flow rates of liquid are 0.6 mL/min, 0.8 mL/min, 1.0 mL/min and 1.2 mL/min. Fig. 8(a) displays a synthetic aperture global rainbow image with the liquid flow of 0.8 mL/min. The features of rainbow pattern are difficult to be observed, and the green pattern is more apparent. The rainbow signals from 200 lines above and below the middle line of each image are normalized and inversed, and the results are averaged to gain the RI and size of each image. The normalization light intensity distribution of synthetic aperture global rainbow signal is shown in the solid lines of Fig. 8(b), and the fitting is in the dotted lines of Fig. 8(b). Compared with the SASRR, all curves are less smooth and the ripple structure is invisible. The fitting which matches well ensures the reliability and accuracy of the SAGRR. The primary range of droplet size is from 10 μm to 60 μm for procession, of which a point for size inversion is selected every 1 μm. The probability density of size distribution is obtained and with the corresponding size, the Sauter mean diameters are gained. Fig. 8(c) demonstrates the size distribution of an images in the experiment with the flow rate of 1.2 mL/min, and the sizes concentrate on 36μm. The droplets generated by the atomizer are relatively uniform in size within deviation of ten microns. The refractive index and the Sauter mean diameters of different flow rates are illustrated in Fig. 8(d). The measured refractive index is close to 1.3337, and the uncertainty is within 8 $\times 10^{-4}$. The droplet diameter increases with flow rate and the diameters are 30.7 μm, 32.8 μm, 33.5 μm and 41.7 μm. The room mean square errors of RI and diameter are 5 $\times10^{-4}$ and 5 μm. Given the SAGRR is a kind of transient droplet measurement and the laser intensity and the exposure time can be adjusted, the SAGRR is capable of measuring high velocity and intensive industrial sprays. Thus, the synthetic aperture global rainbow refractometry successfully measures sprays with different size distributions at the distance of 800 mm, with high stability and accuracy.

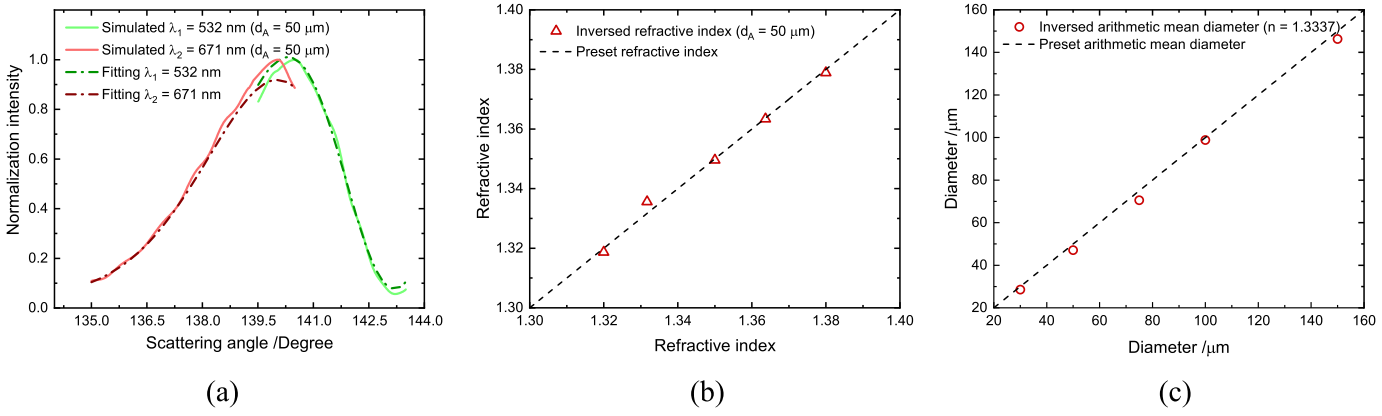

Fig. 6. (a) The simulated synthetic aperture global rainbow signals and the fitting ($d_A = 50$ μm, $n = 1.3337$). (b) The preset and inversed n_{λ_1} with d_A of 50 μm. (c) The preset and inversed Sauter mean diameter with RI of 1.3337.

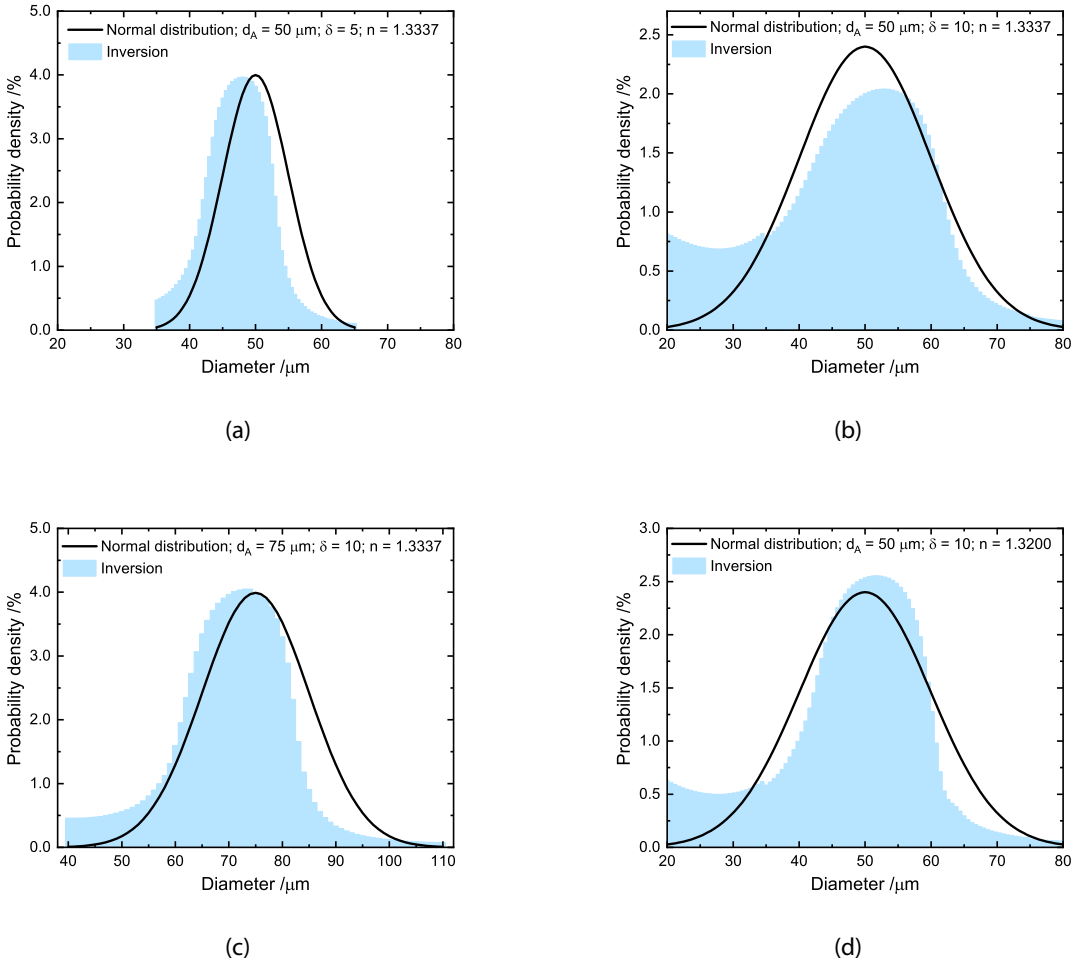

Fig. 7. (a) The comparison of preset and inversed size distribution ($d_A = 50\ \mu m$, $\delta = 5$, n $= 1.3337$). (b) The comparison of preset and inversed size distribution ($d_A = 50\ \mu m$, $\delta = 10$, n $= 1.3337$). (c) The comparison of preset and inversed size distribution ($d_A = 75\ \mu m$, $\delta = 10$, n $= 1.3337$). (d) The comparison of preset and inversed size distribution ($d_A = 50\ \mu m$, $\delta = 10$, n $= 1.3200$).

5. Summary

This work proposes the synthetic aperture standard rainbow refractometry for mono-dispersed droplet measurement, and the synthetic aperture global rainbow refractometry for spray measurement. Both techniques measured transparent, spherical droplets with high accuracy at a longer distance than current rainbow refractometries. The main conclusions are as follow:

1. The synthetic aperture rainbow refractometry significantly increases working distance by synthesizing the aperture of the imaging system, via capturing two rainbow signals generated by two laser beams simultaneously and storing those in different channels of a color image.
2. The formation of the synthetic aperture rainbow signals is modeled. The inversion algorithms of the SASRR and SAGRR are proposed to process rainbow signals.
3. The simulation results certify the reliability of the SASRR with uncertainties of 7×10^{-4} and 2 μm for refractive index and diameter respectively. The monodispersed water and ethanol droplets with size of around 150 μm were surveyed by the SASRR at the distance of 1650 mm, and the mean deviations of refractive index and diameter are both within 8×10^{-4} and 3 μm at room temperature.
4. Through the simulated signals of dispersed droplets with different refractive indices and normal size distributions, the feasibility of the SAGRR is confirmed with uncertainties of 3×10^{-4} and 5 μm for refractive index and diameter. The sprays with diameter of around 35 μm are measured 800 mm away from the synthetic aperture global rainbow refractometry with uncertainty of 8×10^{-4} of refractive index, proving the viability of the SAGRR for spray.

The synthetic aperture standard rainbow refractometry and the synthetic aperture global rainbow refractometry are competent to measure mono-dispersed and dispersed spherical droplets at long distance. The upper and lower limit of the synthetic aperture rainbow refractometry is from 10 μm to 500 μm. This breaks through the limitations of rainbow refractometry and satisfies the aforementioned large scale industrial applications. There will be more possibilities for the synthetic aperture rainbow refractometry if using three or more lasers and combined with one-dimensional rainbow refractometry, phase rainbow refractometry and.

CRediT authorship contribution statement

Yingchun Wu: Resources, Data-curation, Writing-review-editing. **Xinhao Wang:** Methodology, Writing-original-draft. **Dongyan Xu:** Conceptualization. **Xuecheng Wu:** Writing-review-editing.

Declaration of Competing Interest

The authors declare that they have no known competing financial interests or personal relationships that could have appeared to influence

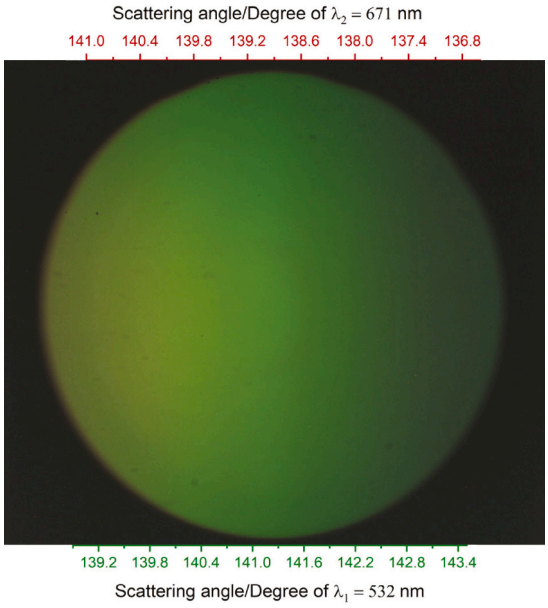

(a)

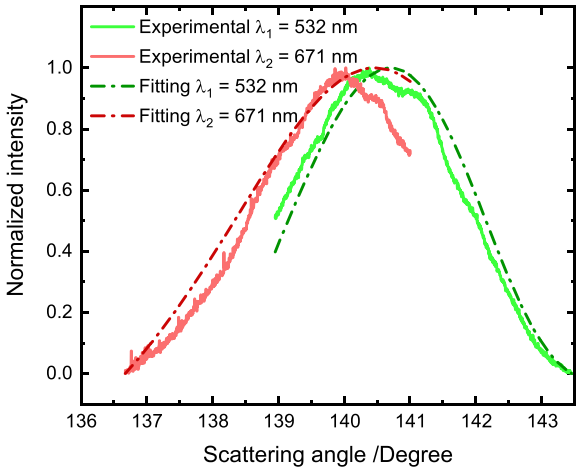

(b)

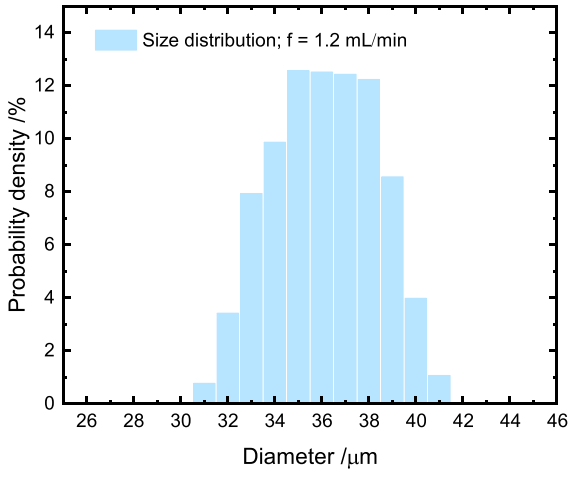

(c)

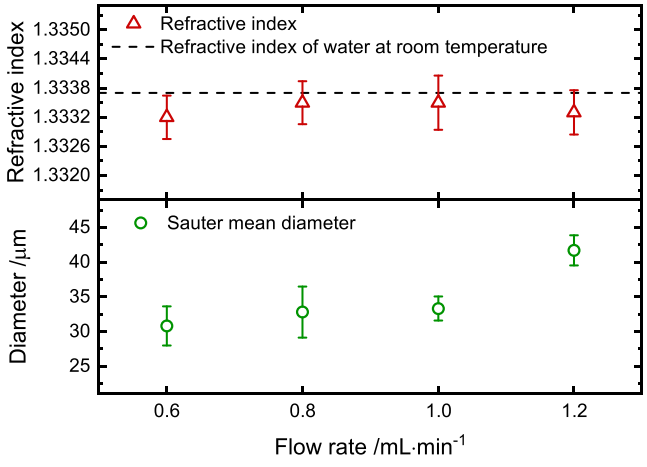

(d)

Fig. 8. (a) The synthetic aperture global rainbow image of spray with the liquid flow rate of 0.8 mL/min. (b) The normalization light intensity distribution and the fitting. (c) The size distribution of an image in the experiment with the flow rate of 1.2 mL/min. (d) The refractive index and Sauter mean diameter of different flow rates.

the work reported in this paper.

Data availability

Data will be made available on request.

Acknowledgment

The authors gratefully acknowledge the support from project supported by National Natural Science Foundation of China (52006193), National Science and Technology Major Project (2017-V-0016–0069, J2019-III-0006–0049), National Key R&D Program of China (Grant No. 2020YFA0405700 and No. 2020YFB0606201).

References

[1] Todd D. Fansler, Scott E. Parrish, Spray measurement technology: a review, Meas. Sci. Technol. 26 (1) (2014) 012002.
[2] J. Shinjo, A. Umemura, Simulation of liquid jet primary breakup: dynamics of ligament and droplet formation, Int. J. Multiph. Flow 36 (7) (2010) 513–532.
[3] C.J. Rutland, Large-eddy simulations for internal combustion engines–a review, Int. J. Engine Res. 12 (5) (2011) 421–451.
[4] William Bachalo, Spray diagnostics for the twenty-first century, Atomization Sprays 10 (3–5) (2000).
[5] Mark Linne, Imaging in the optically dense regions of a spray: a review of developing techniques, Prog. Energy Combust. Sci. 39 (5) (2013) 403–440.
[6] Yasuhiko Iwamoto, K. Noma, O. Nakayama, T. Yamauchi, H. Ando, Development of gasoline direct injection engine, SAE Trans. (1997) 777–793.
[7] V.G. McDonell, G.S. Samuelsen, Measurement of fuel mixing and transport processes in gas turbine combustion, Meas. Sci. Technol. 11 (7) (2000) 870.

[8] Thomas Irvine, Susan Kevdzija, David Sheldon, David Spera, Overview of the icing and flow quality improvements program for the nasa-glenn icing research tunnel, in: 39th Aerospace Sciences Meeting and Exhibit, 2001, pp. 229.
[9] Ludovico Vecchione, Piero De Matteis, An overview of the cira icing wind tunnel, in: 41st Aerospace Sciences Meeting and Exhibit, 2003, pp. 900.
[10] Tatsuya Kawaguchi, Yukihiro Akasaka, Masanobu Maeda, Size measurements of droplets and bubbles by advanced interferometric laser imaging technique, Meas. Sci. Technol. 13 (3) (2002) 308.
[11] A. Garcia-Magarino, S. Sor, R. Bardera, J. Munoz-Campillejo, Interferometric laser imaging for droplet sizing method for long range measurements, Measurement 168 (2021), 108418.
[12] Volker Sick, Michael C. Drake, Todd D. Fansler, High-speed imaging for direct-injection gasoline engine research and development, Exp. Fluids 49 (4) (2010) 937–947.
[13] Philip J. Santangelo, Paul E. Sojka, A holographic investigation of the near-nozzle structure of an effervescent atomizer-produced spray, Atomization Sprays 5 (2) (1995).
[14] Yeon-Jun Choo, Bo-Seon Kang, Measurements of three-dimensional velocities of spray droplets using the holographic velocimetry system, KSME Int. J. 17 (7) (2003) 1095–1103.
[15] J.W. Goodman, D.W. Jackson, M. Lehmann, J. Knotts, Experiments in long-distance holographic imagery, Appl. Opt. 8 (8) (1969) 1581–1586.
[16] W.D. Bachalo, M.J. Houser, Phase/doppler spray analyzer for simultaneous measurements of drop size and velocity distributions, Opt. Eng. 23 (5) (1984), 235583.
[17] Customized ldv systems,https://ila-rnd.com/customized-ldv-systems/.
[18] N. Roth, K. Anders, A. Frohn, Simultaneous measurement of temperature and size of droplets in the micrometer range, J. Laser Appl. 2 (1) (1990) 37–42.
[19] J.P.A.J. Van Beeck, D. Giannoulis, Laurent Zimmer, M.L. Riethmuller, Global rainbow thermometry for droplet-temperature measurement, Opt. Lett. 24 (23) (1999) 1696–1698.
[20] Wu. Xuecheng, Haoyu Jiang, Wu. Yingchun, Jin Song, Gérard Gréhan, Sawitree Saengkaew, Linghong Chen, Xiang Gao, Kefa Cen, One-dimensional rainbow thermometry system by using slit apertures, Opt. Lett. 39 (3) (2014) 638–641.
[21] Can Li, Qimeng Lv, Ning Li, Wu. Yingchun, Wu. Xuecheng, Chunsheng Weng, Cameron Tropea, Planar rainbow refractometry, Opt. Lett. 46 (23) (2021) 5898–5901.
[22] Wu. Yingchun, Jantarat Promvongsa, Sawitree Saengkaew, Wu. Xuecheng, Jia Chen, Gérard Gréhan, Phase rainbow refractometry for accurate droplet variation characterization, Opt. Lett. 41 (20) (2016) 4672–4675.
[23] Wu. Yingchun, Can Li, Jianzheng Cao, Wu. Xuecheng, Sawitree Saengkaew, Linghong Chen, Gérard Gréhan, Kefa Cen, Mixing ratio measurement in multiple sprays with global rainbow refractometry, Exp. Thermal Fluid Sci. 98 (2018) 309–316.
[24] Qimeng Lv, Wu. Yingchun, Can Li, Wu. Xuecheng, Linghong Chen, Kefa Cen, Surface tension and viscosity measurement of oscillating droplet using rainbow refractometry, Opt. Lett. 45 (24) (2020) 6687–6690.
[25] G. Sawitree Saengkaew, JB Blaisot Godard, G. Gréhan, Experimental analysis of global rainbow technique: sensitivity of temperature and size distribution measurements to non-spherical droplets, Exp. Fluids 47 (4) (2009) 839–848.
[26] J.P.A.J. Van Beeck, M.L. Riethmuller, Rainbow phenomena applied to the measurement of droplet size and velocity and to the detection of nonsphericity, Appl. Opt. 35 (13) (1996) 2259–2266.
[27] Yu. Haitao, Xu. Feng, Cameron Tropea, Optical caustics associated with the primary rainbow of oblate droplets: simulation and application in non-sphericity measurement, Opt. Express 21 (22) (2013) 25761–25771.
[28] G.U.O. Xiangdong, L.I.U. Qinglin, L.A.I. Qingren, Y.A.N.G. Shengke, Z.H.A.O. Zhao, Airworthiness compliance verification of aerodynamic flowfield of a large-scale icing wind tunnel, Acta Aerodyn. Sin. 39 (2) (2021) 184–195.
[29] H.M. Nussenzveig, High-frequency scattering by a transparent sphere. ii. theory of the rainbow and the glory, J. Math. Phys. 10 (1) (1969) 125–176.
[30] Richard Bamler, Philipp Hartl, Synthetic aperture radar interferometry, Inverse Prob. 14 (4) (1998) R1.
[31] Philip Laven, Simulation of rainbows, coronas and glories using mie theory and the debye series, J. Quant. Spectrosc. Radiat. Transfer 89 (1–4) (2004) 257–269.
[32] The spectral response of camera,https://docs.baslerweb.com/aca2040-90uc.
[33] Sawitree Saengkaew, Tawatchai Charinpanitkul, Hathaichanok Vanisri, Wiwut Tanthapanichakoon, Loïc Mees, Gérard Gouesbet, Gérard Grehan, Rainbow refractometry: on the validity domain of airy's and nussenzveig's theories, Opt. Commun. 259 (1) (2006) 7–13.
[34] Stefan Kedenburg, Marius Vieweg, Timo Gissibl, Harald Giessen, Linear refractive index and absorption measurements of nonlinear optical liquids in the visible and near-infrared spectral region, Opt. Mater. Express 2 (11) (2012) 1588–1611.
[35] George M. Hale, Marvin R. Querry, Optical constants of water in the 200-nm to 200-μm wavelength region, Appl. Opt. 12 (3) (1973) 555–563.
[36] Elisa Sani, Aldo Dell'Oro, Spectral optical constants of ethanol and isopropanol from ultraviolet to far infrared, Opt. Mater. 60 (2016) 137–141.
[37] Wu. Xuecheng, Qimeng Lv, Wu. Yingchun, Can Li, Kefa Cen, Dual-stream of monodisperse droplet generator, Chem. Eng. Sci. 223 (2020), 115645.